Available online at www.sciencedirect.com
ScienceDirect
Combustion and Flame 153 (2008) 161–172
Combustion and Flame
www.elsevier.com/locate/combustflame

Studies on a heat-recirculating microemitter for a micro thermophotovoltaic system

K.H. Lee, O.C. Kwon *

School of Mechanical Engineering, Sungkyunkwan University, 300 Chunchun-dong, Jangan-gu, Suwon, Kyunggi-do 440-746, Republic of Korea

Received 20 April 2007; received in revised form 7 October 2007; accepted 10 January 2008

Available online 13 February 2008

Abstract

A new microemitter (microcombustor) configuration for a micro thermophotovoltaic system in which thermal energy is directly converted into electrical energy through thermal radiation was investigated experimentally and computationally. The microemitter as a thermal heat source was designed for a 1–10 W power-generating micro thermophotovoltaic system. To satisfy the primary requirements for designing the microemitter (stable burning in the small confinement, maximum heat transfer through the emitting walls, but uniform distribution of temperature along the walls), the present microemitter is cylindrical with an annular-type shield to apply for the heat-recirculation concept. Results show that the heat recirculation substantially improves the performance of the microemitter: the observed and predicted thermal radiation from the microemitter walls indicated that heat generated in the microemitter is uniformly emitted. Thus, the present microemitter configuration can be applied to the practical micro thermophotovoltaic systems without any moving parts (hence frictional losses and clearance problems are avoided). Ratios of the inner radius of the shield to the gap between the shield and microemitter walls and the microemitter wall thickness substantially affect thermal characteristics.

Keywords: Micro thermophotovoltaic system; Microemitter; Microcombustion

1. Introduction

Recently, the demand for light, fast-charging and long-lasting portable power sources to replace current lithium-ion batteries has been increasing due to advances in portable electronic devices such as laptop computers, cellular phones, and camcorders. Miniature or microscale (which will be called *micro* hereafter) power systems using combustion of hydrocarbon fuels are considered one of the alternatives, since they can contain more energy per unit mass than lithium-ion batteries and be quickly charged. Thus, various combustion-based micropower devices have been suggested [1].

Many combustion-based micropower systems are scaled down from macroscale heat engines such as gas turbine and rotary engines [1,2]. However, such micro heat engines involving moving parts seem to be impractical, since overcoming heat and friction losses and the difficulties of fabrication and assembly are considered technological challenges for miniaturizing the systems. In order to avoid such technological difficulties in developing micropower systems

* Corresponding author. Fax: +82 31 290 5889.
E-mail address: okwon@skku.edu (O.C. Kwon).

0010-2180/$ – see front matter
doi:10.1016/j.combustflame.2008.01.003

Nomenclature

A	pre-exponential factor
D	mass diffusivity
D_T	thermal diffusion coefficient
E	energy
E_a	activation energy
d_s	inner diameter of shield
d_w	inner diameter of microemitter
g	acceleration of gravity
h	enthalpy
h_c	heat transfer coefficient
$\vec{J}_i$	diffusive mass flux vector
k	thermal conductivity
l	length of main part of microemitter
$\dot{m}_f$	fuel mass flow rate
M_w	molecular weight
n	temperature exponent
N	number of chemical species in the system
p	pressure
Q	volume flow rate
R_i	net rate of production of species i by chemical reaction
r	radial coordinate
R_u	universal gas constant
Re	Reynolds number
S_h	heat sources
T	temperature
t	time
t_g	gap between shield and microemitter walls
t_w	microemitter wall thickness
$\vec{u}$	flow velocity vector
u_r	velocity component in the radial direction
u_x	velocity component in the axial direction
V	averaged microemitter inlet velocity
X_f	mole fraction of fuel
X_i	mole fraction of species i
x	axial coordinate
Y_i	mass fraction of species i
ϕ	fuel-equivalence ratio
γ	ratio of inner radius of shield to gap between shield and microemitter walls, $(d_s/2)/t_g$
μ	viscosity
ρ	density
τ	stress

involving moving parts, Ahn et al. [3] suggested a micro thermoelectric device that consists of a combustor connected with a heat-recirculating (Swiss-roll type) fuel–air mixture inlet and exhaust outlet assembly for reducing heat losses and thermoelectric elements. Maruta and co-workers also conducted experimental and computational studies on Swiss-roll type and radial microcombustor configurations [4,5]. Federici et al. [6] developed another type of micro thermoelectric device using catalytic combustion for stable burning in a relatively simple combustor configuration. Although the micro thermoelectric power systems could much improve the difficulties of fabrication and assembly, there are still technological challenges: complicated structure for homogeneous gas-phase combustion and a maintenance problem due to easily poisoned catalyst surface for catalytic combustion. Schmidt and co-workers developed radiant micro burners applying the heat-recirculation concept and catalytic combustion for reforming various fuels [7,8].

Considering the technological difficulties of the aforementioned combustion-based micropower systems, a novel micro device should be structurally simple and efficient without moving parts. Thermophotovoltaic (TPV) power generators in which photovoltaic (PV) cells generate electric energy from thermal radiation, similarly to solar cells converting the radiative energy of sunlight into electrical power, have been developed for house heating systems and power suppliers in remote areas and as range extenders in electric cars [9,10]. Due to their simple geometry with no moving parts, TPV power systems are expected to be easily scaled down for micropower generation. Recently, effects of major parameters, including the configuration, wall thickness, and materials of microcombustors and mixture compositions, on microcombustion for TVP energy conversion have been investigated [11]. The investigation, however, was carried out only for hydrogen–air mixtures in a simple cylindrical combustor with a backward-facing step. However, practical use of hydrogen for microcombustors is somewhat questionable due to the fuel storage problem, though hydrogen seems to experience less quenching than hydrocarbon fuels.

In the present investigation, a heat-recirculating but still structurally simple microcombustor (microemitter) for micro TPV power systems using hydrocarbons instead of hydrogen to improve volumetric energy density is suggested to guarantee stable burning in the small confinement while effectively transferring heat into the microemitter wall surface and then uniformly radiating into the PV cells. Identifying the structure of microflames in the microemitter,

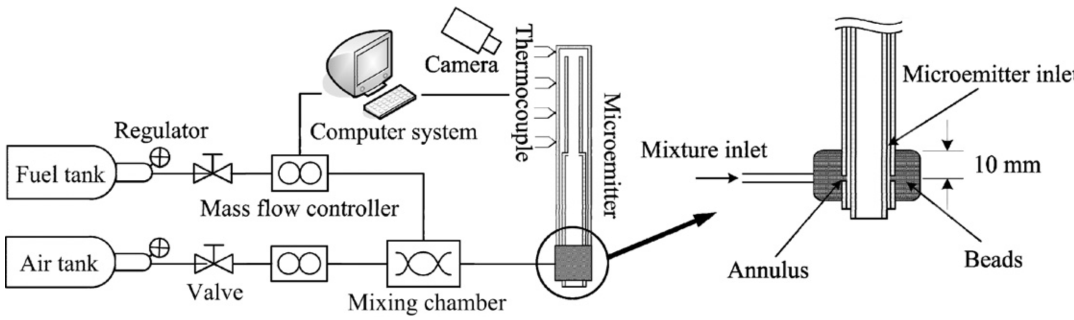

Fig. 1. Schematic of experimental apparatus.

including distributions of fuel and temperature, can help explain the mechanisms of microcombustion. In order to predict the microflame structure, two- or three-dimensional simulations are required.

In view of the above considerations, in the present investigation we aim to design a novel microemitter configuration without catalysts for a micro TPV power system, with the following specific objectives. The first is to determine a basic heat-recirculating configuration that can sustain stable burning for a 1–10 W power-generating micro TPV system. We will determine the proper range of mass flow rates and fuel concentration of supplied hydrocarbon–air premixtures for stable burning and heat transfer. The second is to observe the effects of geometric variations such as the gap between microemitter walls and the wall thickness on combustion characteristics in the microemitter and heat transfer through the microemitter walls. The third is to provide the optimized design conditions from the observations. We shall also examine the structure of microflames in a small confinement based on a CFD simulation with a simplified kinetic mechanism, in order to understand some unique characteristics of microflames and heat transfer through the walls.

The basic configuration of the microemitter with the proper range of mass flow rates and fuel concentration of supplied hydrocarbon–air premixtures, the effects of geometric variations on combustion and heat transfer characteristics, and the optimized design conditions will be subsequently presented, following specification of the experimental and computational methods used during the present investigation.

2. Experimental and computational methods

A diagram of the present experimental apparatus appears in Fig. 1, which consists of a test microemitter (stainless steel, SS304), a fuel–air mixture supply system, thermocouples for measuring temperature distribution on the outer wall surface of the microemitter, and a digital camera (Nikon D70) for recording the radiating microemitter images. In the present study, we focus on demonstrating whether heat recirculation can improve the microemitter performance; thus, stainless steel was used for the test emitter due to easy fabrication, though better materials for emitters, e.g., silicon carbide (SiC), could be considered. Commercial mass flow controllers (Teledyne Hasting Instruments: 100 and 1000 sccm; Alicat Scientific: 2000 sccm) with accuracy ±0.75–1.00% of full scale delivered the combustible mixture to the microemitter: they were commanded by a PC-based program (LabView) that enabled independent control of mixture composition (or fuel-equivalence ratio ϕ) and microemitter inlet velocity V (or volume flow rate Q). The mixture was delivered into the annulus through beads to obtain uniform flow at the microemitter inlet. Temperature distribution on the outer wall surface of the microemitter was measured using K-type thermocouples (bead diameter 250 ± 20 μm) with measurement accuracy ±0.05%. Final results were obtained by averaging measurements of three to four tests for each condition. Experimental uncertainties (95% confidence) for temperature were less than 2.5%. Configurations of designed microemitters will be discussed later.

Flames in the microemitter were obtained by establishing a cold injected flow of a reactive mixture and then igniting the mixture at the exhaust outlet with a spark: once the mixture was ignited, the flames moved backward and were stabilized in the microemitter. Experiments were carried out for propane (C_3H_8, purity >99.5%)–air (21% O_2/79% N_2 in volume) mixtures with $\phi = 0.9$–1.1 and $V = 3.3$ m/s (Reynolds number Re $= 168$, and hence laminar) at temperature $T = 298 \pm 3$ K and atmospheric pressure (NTP). C_3H_8 was chosen as a fuel since it can be liquefied at relatively low pressures and be easily vaporized when mixed with air at NTP; thus, C_3H_8 has the potential for practical use. To evaluate effects of ratios (γ) of the inner radius of a shield ($d_s/2$) for heat recirculation to the gap between the shield and microemitter walls (t_g) and the microemitter wall thickness (t_w)

on the microemitter performance, experiments were carried out for microemitters with $d_\mathrm{s} = 3.0$–4.0 mm, $t_\mathrm{g} = 1.0$–1.5 mm, and $t_\mathrm{w} = 0.5$–1.0 mm.

Microcombustion in microemitters was simulated using a commercially available CFD code, FLUENT 6.2 [12], results from which were analyzed along with those of experimental tests for effectively designing microemitters. The time-dependent ordinary sets of the continuity equation, the cylindrical two-dimensional (cylindrical: r–x, where r and x are the radial and axial coordinates, respectively) Navier–Stokes equations, the energy conservation equation, and the species conservation equations were solved by the finite volume method. The governing equations can be written

$$\frac{\partial\rho}{\partial t} + \frac{\partial}{\partial x}(\rho u_x) + \frac{\partial}{\partial r}(\rho u_\mathrm{r}) + \frac{\rho u_\mathrm{r}}{r} = 0, \tag{1}$$

$$\begin{aligned}
&\frac{\partial}{\partial t}(\rho u_x) + \frac{1}{r}\frac{\partial}{\partial x}(r\rho u_x u_x) + \frac{1}{r}\frac{\partial}{\partial r}(r\rho u_\mathrm{r} u_x) \\
&\quad = -\frac{\partial p}{\partial x} + \frac{1}{r}\frac{\partial}{\partial x}\left[r\mu\left(2\frac{\partial u_x}{\partial x} - \frac{2}{3}(\nabla\cdot\vec{u})\right)\right] \\
&\qquad + \frac{1}{r}\frac{\partial}{\partial r}\left[r\mu\left(\frac{\partial u_x}{\partial r} + \frac{\partial u_\mathrm{r}}{\partial x}\right)\right] + \rho g,
\end{aligned} \tag{2}$$

$$\begin{aligned}
&\frac{\partial}{\partial t}(\rho u_\mathrm{r}) + \frac{1}{r}\frac{\partial}{\partial x}(r\rho u_x u_\mathrm{r}) + \frac{1}{r}\frac{\partial}{\partial r}(r\rho u_\mathrm{r} u_\mathrm{r}) \\
&\quad = -\frac{\partial p}{\partial r} + \frac{1}{r}\frac{\partial}{\partial x}\left[r\mu\left(\frac{\partial u_\mathrm{r}}{\partial x} + \frac{\partial u_x}{\partial r}\right)\right] \\
&\qquad + \frac{1}{r}\frac{\partial}{\partial r}\left[r\mu\left(2\frac{\partial u_\mathrm{r}}{\partial r} - \frac{2}{3}(\nabla\cdot\vec{u})\right)\right] \\
&\qquad - 2\mu\frac{u_\mathrm{r}}{r^2} + \frac{2}{3}\frac{\mu}{r}(\nabla\cdot\vec{u}),
\end{aligned} \tag{3}$$

$$\begin{aligned}
&\frac{\partial}{\partial t}(\rho E) + \nabla\cdot\big(\vec{u}(\rho E + p)\big) \\
&\quad = \nabla\cdot\left(k\nabla T - \sum_i h_i \vec{J}_i + \big(\bar{\bar{\tau}}\cdot\vec{u}\big)\right) + S_\mathrm{h},
\end{aligned} \tag{4}$$

$$\frac{\partial}{\partial t}(\rho Y_i) + \nabla\cdot(\rho\vec{u}Y_i) = -\nabla\cdot\vec{J}_i + R_i, \tag{5}$$

where

$$E = h - \frac{p}{\rho} + \frac{u^2}{2},$$

$$h = \sum_i Y_i h_i,$$

and

$$\vec{J}_i = -\sum_{j=1}^{N-1}\rho D_{ij}\nabla Y_j - D_{T,i}\frac{\nabla T}{T}.$$

The notation of these is described in the Nomenclature. Multicomponent diffusion, thermal diffusion, variable thermochemical properties, and variable transport properties were considered. The CHEMKIN database was used to find the thermochemical properties [13]. For typical test conditions, the thermal radiation from the microemitter wall surface into a virtual PV cell surface was simulated by the surface-to-surface model [14]. C_3H_8 and air (21% O_2/79% N_2 in volume) mixtures were considered with a simplified four-step reversible C_3H_8/O_2 reaction mechanism involving seven species due to Hautman et al. [15], as follows:

$$\begin{aligned}
&C_3H_8 \to \frac{3}{2}C_2H_4 + H_2, \\
&C_2H_4 + O_2 \to 2CO + 2H_2, \\
&CO + \frac{1}{2}O_2 \to CO_2, \\
&H_2 + \frac{1}{2}O_2 \to H_2O.
\end{aligned} \tag{6}$$

The reaction rate of each step is generally described in the modified Arrhenius form, as follows:

$$k = AT^n \exp\left(\frac{-E_\mathrm{a}}{R_\mathrm{u}T}\right). \tag{7}$$

For each reaction, the corresponding Arrhenius parameters—the pre-exponential factor, A, the temperature exponent, n, and the activation energy, E_a—are prescribed.

The governing equations adapting the above submodels were discretized and simultaneously solved [12]. The number of grids was determined through the grid-independence test, varying the number from 10,000 to 50,000, which showed no changes (within 1%) of the results beyond 32,000 grid points. Parabolic flow of a fuel–air mixture (given V and mole fraction of species i (X_i)) at NTP was supplied at the microemitter inlet. Pressure outlet conditions were applied for the exhaust outlet of microemitter: zero gradients of T, X_i, u_x, and u_r. Applied boundary conditions are as follows: no-slip conditions and $dX_i/dr = 0$ on the inside wall of the microemitter and ambient air with heat transfer coefficient $h_\mathrm{c} = 25\ \mathrm{W/(m^2\,K)}$ at $T = 298$ K on the outside wall of the microemitter [3]. Thermal conductivity and specific heat at constant pressure of stainless steel were provided as a function of T [16], while a constant emissivity of 0.5 was applied [17]. The parallel computation system of 16 personal computers (CPU speed 3.0 GHz each) allowed two-dimensional computations with the submodels. Numerical simulations were conducted for the same conditions as those for experiments.

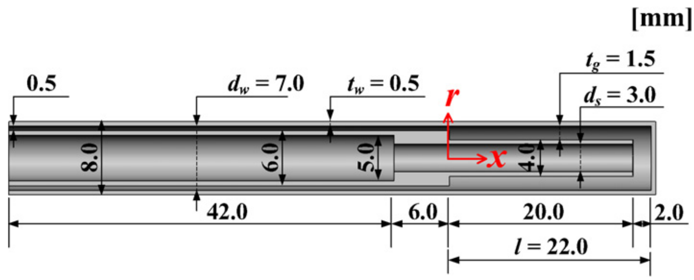

Fig. 2. Configuration of a heat-recirculating microemitter.

3. Results and discussion

3.1. Microemitter configurations

In the present study a microemitter configuration for a 1–10 W power-generating TPV was designed. Assuming that the conversion efficiencies of thermal to electric energies in micro TPV systems are much lower than those for conventional macro-scale TPV, the size of the present microemitter was determined.

In order to use a simple structure but uniformly radiating microemitter, a cylindrical configuration was chosen as the basic geometry of the microemitter. The reason to keep temperature uniform on the microemitter wall surface is that large temperature gradients significantly degrade the performance of micro TPV systems. For practical purposes, it is best to reduce the temperature difference along the outer wall surface of microemitter as much as possible. Thus, the heat-recirculation concept, extracting heat from exhaust gas for preheating fresh fuel–air mixtures, was applied for the present microemitter. Fig. 2 shows a basic microemitter configuration and major dimensions (inner diameter of microemitter $d_w = 7.0$ mm, $d_s = 3.0$ mm, $t_g = 1.5$ mm ($\gamma = 1.0$), $t_w = 0.5$ mm, and length of the main part of the microemitter $l = 22.0$ mm). An annular-type shield was installed in the microemitter in order to adopt the heat-recirculation concept: exhaust gas burned between the shield and microemitter walls turns around the shield near the closed end of the microemitter, and then the exhaust gas preheats a fresh mixture supplied to the microemitter across the shield wall. When the preheated fuel–air mixture is burned, enhanced uniformity of temperature is expected [18].

Fig. 3 shows a conceptual design for a micro TPV system: the microemitter is surrounded with an annular vacuum chamber, dielectric filters, PV cells, and cooling fins. For the virtual micro TPV system, the temperature distribution along the wall surface of the microemitter that is covered by PV cells should be as uniform as possible. The present design concerned only the microcombustor configuration (not the whole micro TPV system); thus, experiments and computations were conducted for the microemitter surrounded with atmosphere at NTP, except for an additional computation to estimate the amount of thermal radiation from the microemitter wall into virtual PV cells in vacuum.

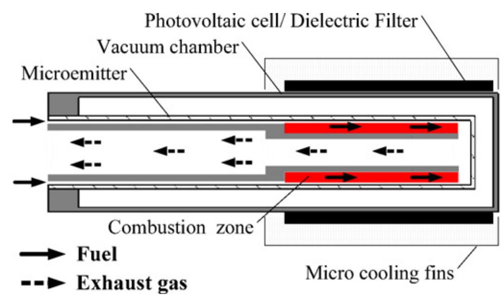

Fig. 3. A conceptual design for a micro TPV power system.

Prior to examining the heat-recirculating effects, the temperature distribution along the outer wall surface of a simple cylindrical microemitter of $d_w = 7.0$ mm, $l = 22.0$ mm, and $t_w = 0.5$ mm without the heat recirculation (the same as the configuration and dimensions in Fig. 2 but with no cap on the right end of the microemitter) for a C_3H_8–air mixture of $\phi = 1.0$ and $V = 2.4$ m/s at NTP was measured and is shown in Fig. 4, along with the radiating image. The inlet velocity of the mixture was determined at the maximum value where a flame could be stabilized in the microemitter. Along the wall surface of the main part of the microemitter that would be surrounded by the PV cells ($x/l = 0$–1 for the present coordinate system in Fig. 2), the temperature drops by 325 K, which is equivalent to a temperature gradient of 15 K/mm, showing nonuniform radiation. Thus, as expected, the direct burning without heat recirculation is not suitable for the microemitter application.

Fig. 5 shows the temperature distribution along the outer wall surface of the heat-recirculating microemitter shown in Fig. 2 for a C_3H_8–air mixture with $\phi = 1.0$ and $V = 3.3$ m/s at NTP, along with the radiating image. The inlet velocity of the mixture was determined by controlling it to establish a flame at a proper position for various conditions. Compared to

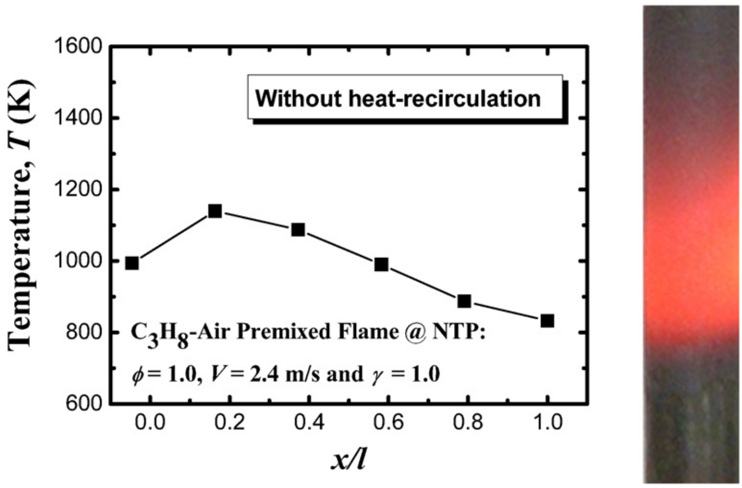

Fig. 4. Measured temperature distribution along the outer wall surface of the microemitter without heat recirculation ($d_w = 7.0$ mm, $l = 22.0$ mm, and $t_w = 0.5$ mm) and a radiating image for a C_3H_8–air mixture with $\phi = 1.0$ and $V = 2.4$ m/s at NTP.

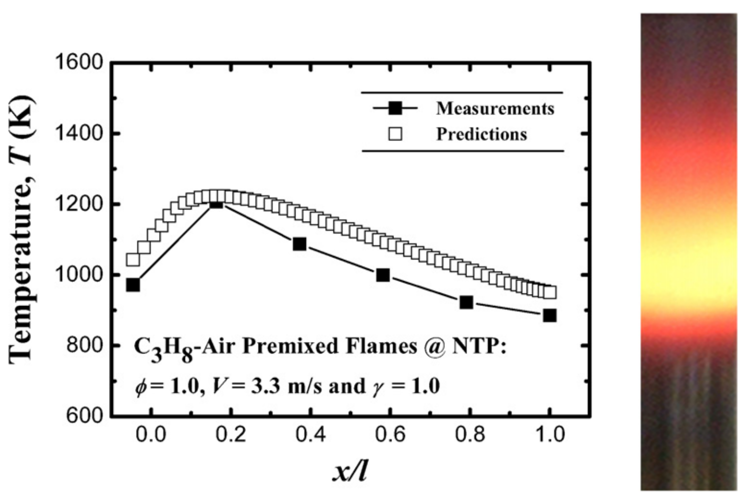

Fig. 5. Measured and predicted temperature distributions along the outer wall surface of the heat-recirculating microemitter ($d_w = 7.0$ mm, $l = 22.0$ mm, $\gamma = 1.0$, and $t_w = 0.5$ mm) and a radiating image for a C_3H_8–air mixture with $\phi = 1.0$ and $V = 3.3$ m/s at NTP. Predictions based on the reaction mechanism due to Hautman et al. [15].

the temperature distribution without heat recirculation from exhaust gas (Fig. 4), the temperature distribution with the recirculation shows a reduced temperature gradient along the microemitter wall, 11 K/mm. As shown in the radiating image, however, the temperature uniformity does not seem to be high enough for the best performance of the micro TPV system. Thus, geometric variations for the heat recirculation effect to be maximized will be considered later.

Predicted distributions of temperature and mole fraction of fuel (X_f) in the heat-recirculating microemitter are shown in Fig. 6. The distributions are displayed in the same coordinate system as shown in Fig. 2. Compared to the measured one, the predicted temperature on the microemitter wall is somewhat higher (also shown in Fig. 5). However, the quantitative difference is less than 8%, which is usually acceptable for most computational predictions, showing that the tendencies of the temperature distribution are very similar to each other and that the predicted temperature drop at $x/l = 0$–1 along the microemitter wall is still similar to the measurement. These observations justify the present approach to microemitter design combining measurements with computations. Predicted distribution of fuel concentration shows that fuel starts to be consumed relatively upstream and immediately disappears, implying that the residence time of the supplied mixture in the microemitter is

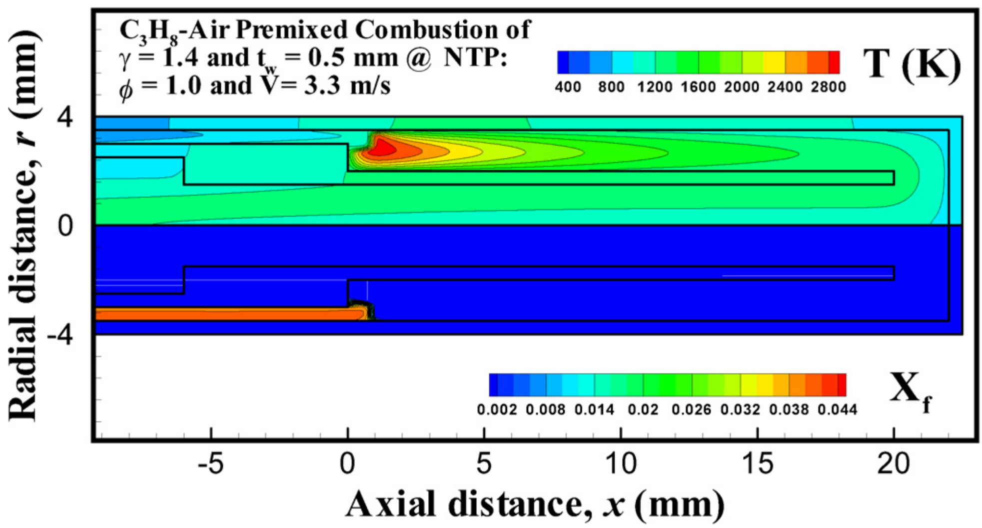

Fig. 6. Predicted distributions of temperature and mole fraction of fuel in the heat-recirculating microemitter ($d_w = 7.0$ mm, $l = 22.0$ mm, $\gamma = 1.0$ and $t_w = 0.5$ mm) for a C_3H_8–air mixture of $\phi = 1.0$ and $V = 3.3$ m/s at NTP. Predictions based on the reaction mechanism due to Hautman et al. [15].

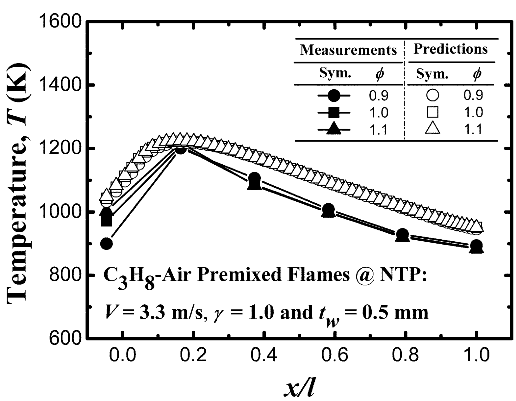

Fig. 7. Measured and predicted temperature distributions along the outer wall surface of the heat-recirculating microemitter (d_w = 7.0 mm, l = 22.0 mm, γ = 1.0, and $t_w = 0.5$ mm) for C_3H_8–air mixtures with $\phi = 0.9$, 1.0, and 1.1 and $V = 3.3$ m/s at NTP. Predictions based on the reaction mechanism due to Hautman et al. [15].

long enough for localized burning, which results in the somewhat nonuniform radiation shown in Fig. 5. As discussed in Fig. 3, showing a virtual micro TPV system, the temperature distribution along the wall surface of microemitter that is covered by PV cells should be as uniform as possible.

Finally, the effects of ϕ on the temperature distribution along the microemitter wall were investigated and are shown in Fig. 7. The experiments were conducted for C_3H_8–air mixtures with $\phi = 0.9$, 1.0 (the baseline condition shown in Figs. 5 and 6), and 1.1 and $V = 3.3$ m/s at NTP. The temperature distributions for various ϕ are similar to each other, except upstream, where the highest temperature is observed under slightly fuel-rich condition. Predicted distributions of temperature and mole fraction of fuel in the microemitter for $\phi = 0.9$ and 1.1 are shown in Fig. 8. Again, a similar temperature distribution is observed for all the fuel-equivalence ratios. Thus, all the experiments in the present study were conducted only for $\phi = 1.0$.

3.2. *Effects of geometric variations*

The experiments were systematically conducted to investigate the effects of the ratio of the inner radius of the shield for heat recirculation to the gap between the shield and microemitter walls and the microemitter wall thickness on the temperature distribution along the microemitter wall for effective thermal radiation.

The effects of the ratio of the inner radius of the shield for heat recirculation to the gap between the shield and microemitter walls on the temperature distribution along the microemitter wall are shown in Fig. 9. The experiments were conducted for a C_3H_8–air mixture of $\phi = 1.0$ and $V = 3.3$ m/s at NTP in microemitters of $\gamma = 1.0$ (the baseline configuration shown in Fig. 2), 1.4, and 2.0. The temperature distribution becomes more uniform and the location where peak temperature is observed shifts downstream with increasing γ. The temperature gradients at $x/l = 0$–1 along the microemitter wall for $\gamma = 1.4$ and 2.0 are 10 and 3 K/mm, respectively (cf. 11 K/mm for $\gamma = 1.0$). This tendency of temperature distribution with varying γ is well predicted, though all the values are overestimated. Predicted distributions of temperature and mole fraction of fuel in the microcombustor for

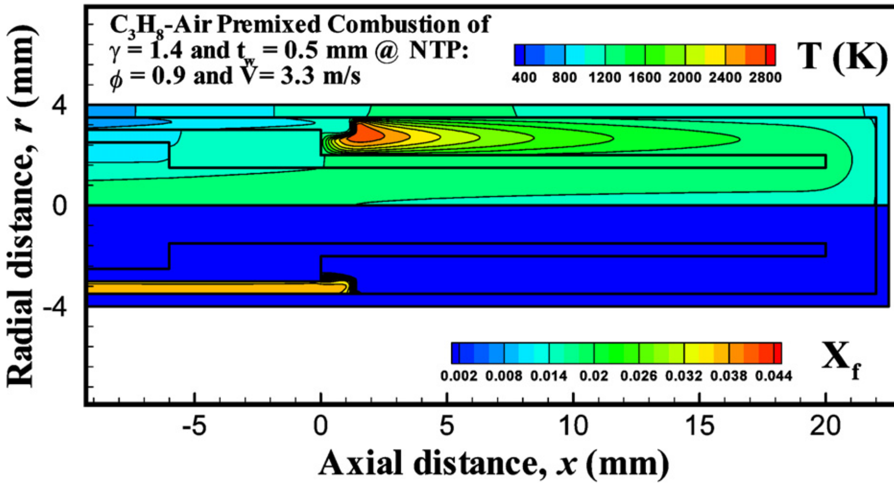

(a)

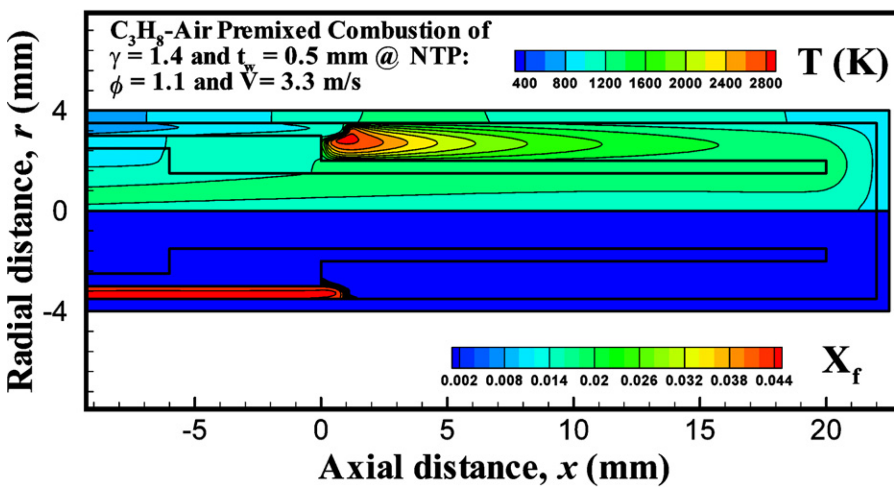

(b)

Fig. 8. Predicted distributions of temperature and mole fraction of fuel in the heat-recirculating microemitter ($d_w = 7.0$ mm, $l = 22.0$ mm, $\gamma = 1.0$, and $t_w = 0.5$ mm) for C_3H_8–air mixtures with $\phi =$ (a) 0.9 and (b) 1.1, and $V = 3.3$ m/s at NTP. Predictions based on the reaction mechanism due to Hautman et al. [15].

$\gamma = 2.0$ are shown in Fig. 10, along with the radiating image. Compared to the baseline condition in Figs. 5 and 6, the enhanced temperature uniformity on the wall surface of the main part of the microemitter with increasing γ is confirmed from the uniformly radiating image. The predicted distribution of fuel concentration shows that fuel starts to be consumed downstream and gradually disappears. This is observed since the residence time of the supplied mixture in the microemitter is much shorter due to a reduced cross-sectional area relative to that for the baseline condition in Fig. 6. Also, still hot burned gas turns around the shield, extending the thermal radiation into ambient air further downstream. Thus, the somewhat nonuniform radiation shown in Fig. 5 has been substantially improved.

The averaged measured gas temperatures at the exhaust outlets of microemitters for $\gamma = 1.0$ and 2.0 are, respectively, 723 and 900 K, implying that more heat is recovered from the heat recirculation for lower γ. This is also confirmed from the predicted exhaust gas temperatures and the amounts of heat transferred from the exhaust gas into the fresh mixtures, which could be calculated from Figs. 6 ($\gamma = 1.0$) and 10 ($\gamma = 2.0$). However, more recovered heat with lower γ is overwhelmed by nonuniform radiation, as shown in Fig. 6, due to localized combustion, i.e., a longer residence time and a shorter region of hot burned gas after turning around the shield.

These observations suggest that stable and uniform burning in the microemitter is most favorable at enhanced ratios of the inner radius of the shield to the gap between the shield and microemitter walls within the gap allowed for stable burning, i.e., beyond a quenching distance at a given fuel concentration and temperature condition, though more consideration is needed for obtaining regular radiation, even with more heat recovery.

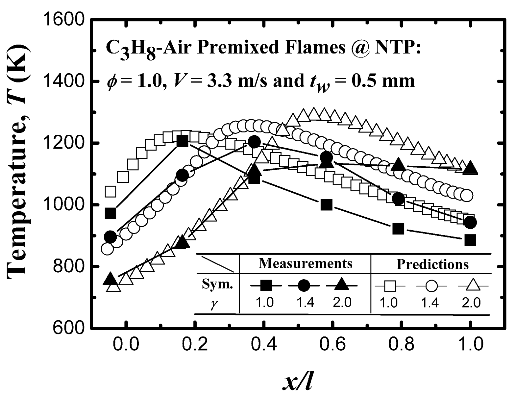

Fig. 9. Effects of γ on temperature distribution along the outer wall surface of the heat-recirculating microemitter ($d_W = 7.0$ mm, $l = 22.0$ mm, and $t_W = 0.5$ mm) for a C_3H_8–air mixture with $\phi = 1.0$ and $V = 3.3$ m/s at NTP: $\gamma = 1.0$, 1.4, and 2.0. Predictions based on the reaction mechanism due to Hautman et al. [15].

The effects of microemitter wall thickness on the temperature distribution along the microcombustor wall are shown in Fig. 11. The experiments were conducted for a C_3H_8–air mixture of $\phi = 1.0$ and $V = 3.3$ m/s at NTP in microemitters of $\gamma = 2.0$ and $t_W = 0.5$ and 1.0 mm. The tendency of the temperature distribution for thin and thick walls is similar to each other, showing almost the same temperature gradient at $x/l = 0$–1 along the microemitter wall; however, the temperature is much reduced with increasing t_W. This tendency of reduced temperature with increasing t_W is well predicted, though all the values and the gradients are overestimated. Predicted distributions of temperature and mole fraction of fuel in the microemitter for $t_W = 1.0$ mm are shown in Fig. 12, along with the radiating image. Although the temperature uniformities along the wall surface for microemitters with thin and thick walls are similar to each other, the radiating image for the microemitter with the thicker wall looks less uniform. However, this is observed just due to the reduced temperature condition: the microemitter wall radiates at almost the boundary of the visible wavelength region. The reduced temperature with increasing t_W implies that the heat conduction in the axial direction plays an important role in the microemitter. Since the axial heat conduction compared to the radial heat transfer across the wall increases with increasing t_W, heat losses through

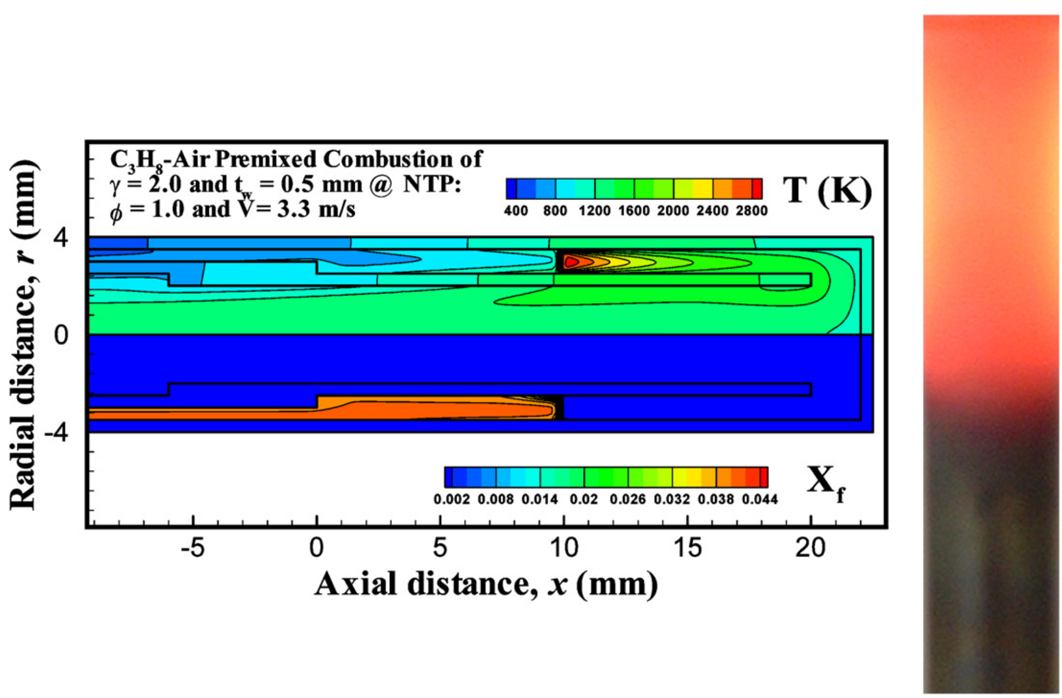

Fig. 10. Effects of γ on distributions of temperature and mole fraction of fuel in the heat-recirculating microemitter ($d_W = 7.0$ mm, $l = 22.0$ mm, and $t_W = 0.5$ mm) and a radiating image for a C_3H_8–air mixture with $\phi = 1.0$ and $V = 3.3$ m/s at NTP: $\gamma = 2.0$. Predictions based on the reaction mechanism due to Hautman et al. [15].

the wall increase. This suggests that stable combustion in the microemitter is most favorable for thinner walls within the thickness allowed for fabrication and structural strength. The predicted distribution of fuel concentration is similar to that for the microemitter with the thinner wall shown in Fig. 6, except for the reduced temperature.

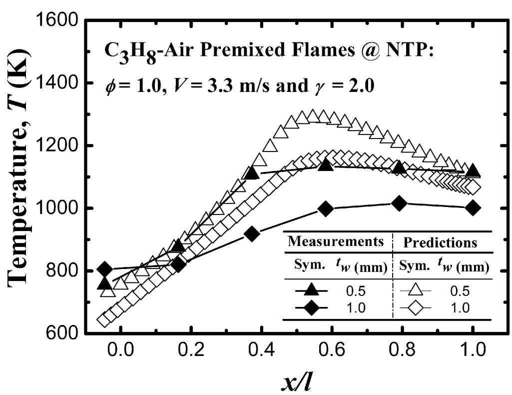

Fig. 11. Effects of t_w on temperature distribution along the outer wall surface of the heat-recirculating microemitter ($d_w = 7.0$ mm, $l = 22.0$ mm, and $\gamma = 2.0$) for a C_3H_8–air mixture with $\phi = 1.0$ and $V = 3.3$ m/s at NTP: $t_w = 0.5$ and 1.0 mm. Predictions based on the reaction mechanism due to Hautman et al. [15].

3.3. The optimized design conditions

So far we have investigated effects of geometric variations on the microemitter performance. Considering that fuel-equivalence ratios around the stoichiometric condition do not much affect performance and that inlet velocities of supplied mixtures can be determined just depending on the target power, we suggest that stable and uniform burning in the microemitter is most favorable at enhanced ratios of the inner radius of shield to the gap between the shield and microemitter walls within the gap allowed for stable burning, i.e., beyond a quenching distance at a given fuel concentration and temperature condition, and for thinner walls within the thickness allowed for fabrication and structural strength. Of course, further considerations are needed to obtain really optimized design condition: e.g., a trade-off between regular radiation and more heat recovery, a choice of materials of microemitter wall, which should be determined depending on target bands of radiating PV cells (e.g., broadband or selective band), and a choice of materials of shield wall that can improve heat recirculation.

Among the present test conditions and configurations of microemitters, the optimized design condition is to burn a C_3H_8–air mixture of $\phi = 1.0$ and $V = 3.3$ m/s (fuel mass flow rate $\dot{m}_f = 2.43 \times 10^{-6}$ kg/s) at NTP in microemitters of $d_w = 7.0$ mm,

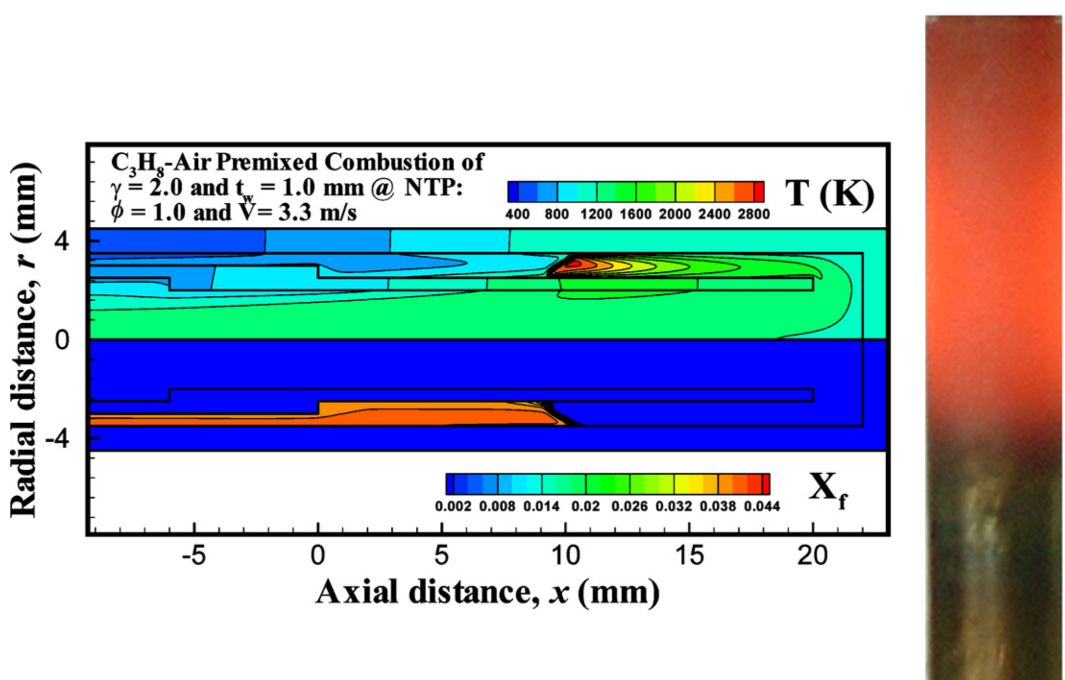

Fig. 12. Effects of t_w on distributions of temperature and mole fraction of fuel in the heat-recirculating microemitter ($d_w = 7.0$ mm, $l = 22.0$ mm, and $\gamma = 2.0$) and a radiating image for a C_3H_8–air mixture with $\phi = 1.0$ and $V = 3.3$ m/s at NTP: $t_w = 1.0$ mm. Predictions based on the reaction mechanism due to Hautman et al. [15].

$d_s = 4.0$ mm, $t_g = 1.0$ mm ($\gamma = 2.0$), $t_w = 0.5$ mm, and $l = 22.0$ mm. For the condition, thermal radiation from the microemitter wall surface into the virtual PV cell surface in vacuum was simulated to obtain the amount of delivered energy and then to roughly estimate the final output power. The predicted microemitter efficiency is 39.5% and the estimated output power is 3.6 W, assuming a microemitter wall emissivity of 0.5 (though the emissivity varies depending on temperature) [17] and a PV cell efficiency of 10% [19]. From the output power, the overall efficiency can be estimated to be 3.2% for the micro TPV system.

As mentioned earlier, the emitter efficiency and the output power are expected to be significantly improved by replacing the emitter materials, e.g., SiC, due to the enhanced emissivity (0.9 [17]). Of course, the heat recovery can be reduced by replacing the shield materials with SiC (but it also depends on the shield wall thickness). The net effects of replacing the materials can be completely understood when the simulation is carried out. Also, it should be noted that the results using SiC for both the microemitter and shield walls can be different from those using SiC for the microemitter wall and stainless steel for the shield wall. The microemitter and overall efficiencies and estimated output power of the microemitter using SiC for the microemitter wall and stainless steel for the shield wall are respectively 52.8%, 4.3%, and 4.8 W for the same conditions as the present optimized ones, showing that the efficiencies are approximately 30% enhanced just by replacing the materials.

4. Conclusions

A new microemitter configuration for a micro thermophotovoltaic system in which thermal energy is directly converted into electrical energy through thermal radiation was investigated experimentally and computationally. The microemitter as a thermal heat source was designed for a 1–10 W power-generating micro thermophotovoltaic system. The major conclusions of the study are as follows:

1. To satisfy the primary requirements for designing a microemitter, i.e., stable burning in the small confinement and maximum heat transfer through the emitting walls, but uniform distribution of temperature along the walls, the present microemitter is cylindrical with an annular-type shield so that a heat recirculation concept can be applied.
2. For the optimized design conditions, the heat recirculation substantially improves the performance of the microemitter: the observed and predicted thermal radiation from the microemitter wall indicated that heat generated in the microemitter was uniformly emitted.
3. Thermal characteristics along the microemitter wall were improved with increasing ratios of the inner radius of the shield to the gap between the shield and microemitter walls, though the total recovered heat was reduced with the enhanced ratios.
4. Thermal characteristics along the microemitter wall were improved with decreasing wall thickness of the microemitter within the thickness allowed for fabrication and structural strength.
5. Predictions for a micro TPV system including virtual PV cells under a typical present test condition showed that the overall efficiency and the output power are 3.2% and 3.6 W, respectively. Replacing the microemitter wall materials with practical SiC, the performance has been much improved: the overall efficiency and the output power are 4.3% and 4.2 W, respectively.

Acknowledgment

This work was supported by the Korea Energy Management Corporation, Korea, under Grant 2004-03-0012-0-000.

References

[1] C. Fernandez-Pello, Proc. Combust. Inst. 29 (2002) 883–899.
[2] A. Mehra, A.A. Ayon, I.A. Waitz, M.A. Schmidt, J. Microelectromech. Syst. 8 (1999) 152–160.
[3] J. Ahn, C. Eastwood, L. Sitzki, P.D. Ronney, Proc. Combust. Inst. 30 (2004) 2463–2472.
[4] N.I. Kim, S. Aizumi, T. Yokomori, S. Kato, T. Fujimori, K. Maruta, Proc. Combust. Inst. 31 (2007) 3243–3250.
[5] S. Kumar, K. Maruta, S. Minaev, J. Micromech. Microeng. 17 (2007) 900–908.
[6] J.A. Federici, D.G. Norton, T. Bruggemann, K.W. Voit, E.D. Wetzel, D.G. Vlachos, J. Power Sources 161 (2006) 1469–1478.
[7] J. Redenius, L.D. Schmidt, AlChE J. 47 (2001) 1177–1184.
[8] E.C. Wanat, K. Venkataraman, L.D. Schmidt, Appl. Catal. A 276 (2004) 155–162.
[9] T. Aicher, P. Kästner, A. Gopinath, A. Gombert, A.W. Bett, T. Schlegl, C. Hebling, J. Luther, in: A. Gopinath, T.J. Coutts, J. Luther (Eds.), Thermophotovoltaic Generation of Electricity, Sixth Conference on Thermophotovoltaic Generation of Electricity TPV6, American Institute of Physics, Melville, NY, 2004, pp. 71–78.
[10] G. Colangelo, A. de Risi, D. Laforgia, Energy Convers. Manage. 47 (2006) 1192–1206.
[11] J.F. Pan, J. Huang, D.T. Li, W.M. Yang, W.X. Tang, H. Xue, Appl. Therm. Eng. 27 (2007) 1089–1095.

[12] Fluent Inc., Fluent 6.2 User's Guide, Fluent Inc., Lebanon, NH, 2001.
[13] R.J. Kee, F.M. Rupley, J.A. Miller, The CHEMKIN Thermodynamic Data Base, Report No. SAND87-8215B, Sandia National Laboratories, 1992.
[14] R. Siegel, J.R. Howell, Thermal Radiation Heat Transfer, fourth ed., Hemisphere Publishing Corp., Washington, DC, 1992, pp. 722–729.
[15] D.J. Hautman, F.L. Dryer, K.P. Schug, I. Glassman, Combust. Sci. Technol. 25 (1981) 219–235.
[16] D. Peckner, I.M. Bernstein, Handbook of Stainless Steels, McGraw–Hill, New York, 1987, chap. 19, pp. 18–26.
[17] Z.W. Li, S.K. Chou, C. Shu, W.M. Yang, J. Micromech. Microeng. 15 (2005) 207–212.
[18] K.H. Lee, O.C. Kwon, Solid State Phenomena 120 (2007) 135–140.
[19] M.A. Green, K. Emery, D.L. King, Y. Hisikawa, W. Warta, Prog. Photovoltaics Res. Appl. 14 (2006) 45–51.